

FIG. 1. The GHz non-linear interference experiment. (a) Schematic of the experiment, as described in the main text. TPS (gold) are used to reconfigure the circuit and offset the CDM phase to minimise the modulation depth required for nonlinear interference. The CDM is depicted by the red/blue box in the lower arm of the interferometer. The reconfigurability of AMZI1 and AMZI2 allows for comparison between nonlinear interference between sources and classical interference in a Mach-Zehnder. (b) Microscope image the photonic integrated circuit used in the experiment.

at measurement. Nonlinear interference between four-wave mixing sources [13] outputs a coincidence detection described by the fringe,

$$f(\phi_p) = \frac{1}{2}(1 + v(R) \cos(n\phi_p + \Phi_0)) \quad (2)$$

where $n = 2$, and Φ_0 captures all other phase terms. $v(R) = 2R/(1 + R^2)$ represents the visibility in terms of the ratio $R = P_2/P_1$ of the probabilities of pair production in each source. The fringe expected from a Mach-Zehnder interferometer is of the same form, but $n = 1$. This difference in fringe frequency is from the SFWM phasematching condition for degenerate pump photons,

$$\phi = 2\phi_p + \phi_i + \phi_s. \quad (3)$$

Therefore, the signature of nonlinear interference between SFWM sources is the doubling of fringe period, compared to a classical linear interferometer fringe.

The photonic integrated circuit used is shown in Fig. 1. It is of in-house design and fabricated by commercially outsourcing to IMEC using their ISIPP50G silicon photonic platform [27]. The photonic circuit is mounted on an in-house designed printed circuit board (PCB) that

carries signals for TPS and the CDM. Temperature stability is maintained using a Peltier element and PID controller (Arroyo 5240).

To operate the chip as a nonlinear interferometer, a continuous wave (CW) laser (Rio Orion), tuned to 1544.61 nm and amplified with an erbium doped-fiber amplifier (Pritel), is coupled to the photonic chip via a fibre polarisation controller (PC), a v-groove fibre array and grating coupler. On chip, the pump is split into two paths with a Mach-Zehnder interferometer (MZI1), tuned to 50:50 beamsplitting to balance power between sources. Asymmetric Mach-Zehnder interferometers with path length difference $\Delta L = 90\mu\text{m}$ are used as add-drop filters with a free-spectral range of ~ 6.4 nm to discard the pump after first source (AMZI-1), and multiplex photon pairs into the second source (AMZI-2). Each photon pair source is a ~ 1.1 cm spiral of single waveguide [28]. Photons are coupled off-chip via a grating coupler and separated into signal and idler channels using fibre based dense-wavelength-division multiplexers (DWDM). Superconducting nanowire single photon detectors (SNSPD, Photonspot, $\sim 85\%$ system efficiency) detect the photons. All TPS are driven by commercial multichannel voltage sources (Qontrol Q8iv). The CDM is driven with signals from an arbitrary waveform generator (AWG, Tektronix 70001A), amplified through an RF voltage amplifier (SHF 810). A bias tee (SHF BT45) is used to combine the RF signal and a DC bias from a benchtop power supply. A TPS in the upper depicted path (without the CDM) is used to minimise coincidences when no RF signal is applied to the CDM.

We verified non-linear interference occurs by comparison with a classical interference fringe on the same device. The chip is configured for classical interference by setting AMZI-1 to perform the identity operation and AMZI-2 to act as a 50:50 beamsplitter. For simplicity, the classical interference is measured by monitoring pump power at the device output. Fig 2 shows raw and fitted data for classical linear interference and for coincidences output from the NLI configuration, in both cases scanning only the TPS in the upper arm.

We demonstrated quantum interference modulated by the CDM. With the chip in its NLI configuration, the CDM is driven with a square wave generated by AWG at 10 MHz and 1 GHz. The driving signal and CDM are impedance matched with a $50\ \Omega$ termination (Smiths Interconnect) wirebonded directly to the photonic chip. The heat dissipated by this termination prevents direct characterisation of the modulator V_π due to thermal crosstalk. We therefore apply a small RF signal (300 mV at 100 kHz) to the modulator while the chip is configured for classical interference and extrapolate V_π assuming a linear voltage-phase relationship. This provides a small-signal estimate of $V_\pi = 7.99 \pm 0.02$ V.

We observe coincidence rates from the device of ~ 100 counts per second. The probability of observing a co-

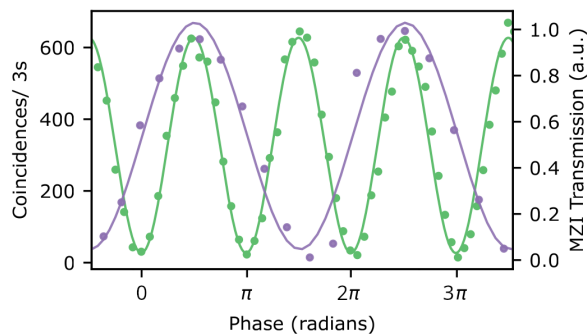


FIG. 2. Linear and nonlinear interference with TPS. Purple data and line of fit from Eq. 2 ($n = 1$) correspond to classical characterisation on right axis. Quantum interference data is plotted in green, with a line of fit from Eq. 2 ($n = 2$). Classical and background subtracted quantum interference display visibilities of 99% and $(96 \pm 1)\%$ respectively.

incidence within any given interval is given by $\langle n \rangle e^{-n}$, where $\langle n \rangle$ is the average coincidence rate in the same interval. Therefore, the probability of observing a coincidence within any given cycle of the modulation is very small, precluding a direct measurement of the interference with GHz driving signals. We therefore attempt to correlate the driving signal with the distribution of coincidences in time by analysing timetags modulo the period of the driving signal. Fig. 3 depicts this analysis.

We synchronise the SNSPD timing logic (Swabian Instruments) with the AWG using a common 10 MHz clock. We note that while the AWG and timetagger clock are synchronised, there is an unknown offset of up to $\frac{1}{2\Omega}$ between the driving signal and the coincidence data, where Ω is the driving frequency. To account for this we offset the photon time tags over a range of $\Delta t = \pm \frac{1}{4\Omega} = \pm \frac{1}{4}T$, which is half the period of the drive waveform. We expect a square wave modulation in the coincidence data, and therefore as this offset is swept we expect the convolution of two square wave, which is a triangle wave peaked at the maximum coincidence visibility. Fig. 4 shows the correlation between the modulation signal and the coincidence data where we have normalised the timetags to zero offset. We compute the interference visibility by summing coincidence counts from the high and low modulator states. We observe (Fig. 4) a raw visibility of $(78 \pm 1)\%$ and $(74 \pm 2)\%$ at 10 MHz and 1 GHz. We estimate the accidental coincidence rates by summing counts outside the histogram peak and dividing by the number of bins. This gives corrected visibilities of $(90 \pm 1)\%$ and $(89 \pm 1)\%$. The single photon counts also vary with ϕ_p , although the fringe visibility is limited by detector dark counts, any distinguishing information between sources such as loss and other photon generation not contained within spiral waveguide arms of the NLI [13]. The maximum observed single photon fringe visibility of $4.41 \pm 0.07\%$ implies a total loss ≈ -13.5 dB.

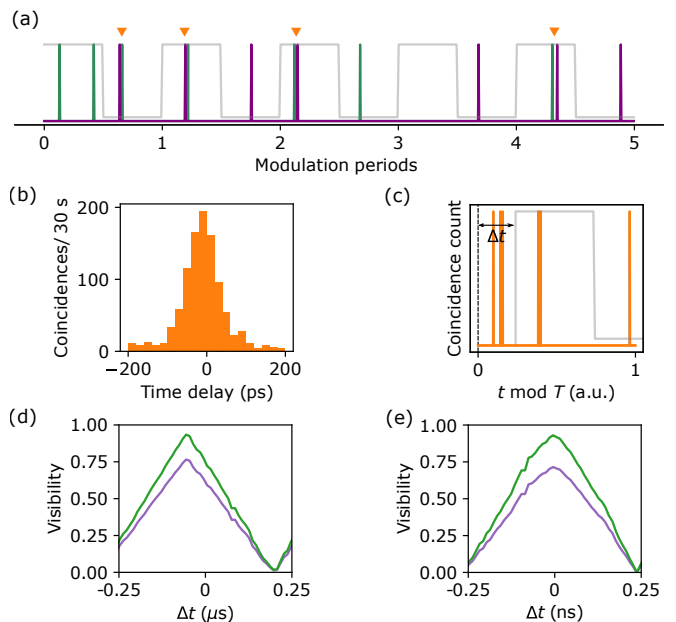


FIG. 3. Coincidence counting of photon pairs. (a) Simulated data illustrating photon coincidences identified between 2 detection channels. Signal and idler pairs (green and purple) are recorded as a coincidences (red) when the delay between channels is less than a predetermined threshold. A square wave driving signal of period T that modulates coincidence rates is overlaid in grey. (b) Coincidences are recorded as a histogram showing the delay between channels with a sign given by the order of timetag events. The absolute timing reference of each timetag is typically discarded. (c) Coincidences may also be located in time by taking the midpoint of timetags from corresponding channels. This data can then be processed modulo T (up to some constant delay) to correlate with the periodic signal used to drive the CDM. (d, e) Coincidence visibility with 10 MHz (d) and 1 GHz (e) modulation as the offset Δt is applied to the time series of coincidence data, divided modulo the waveform period (see main text). Raw data is purple. Background-subtracted data is green. Maximum visibility corresponds to data displayed in Fig. 4.

We measure 6.5 dB loss in each spiral, and attribute the remaining ~ 0.5 dB loss to waveguide and AMZI transmission.

We attribute the limited coincidence visibility to a number of causes. The low-frequency, small-signal value of the voltage for π -phase, V_π , only gives an estimate as the phase shifting efficiency rolls off with frequency due to impedance mismatch with the modulator electrodes, or velocity mismatch to the optical signal. The values we used were determined empirically by halving V_π and then scanning in steps of 50 mV to maximise fringe visibility. A more accurate estimate of $V_\pi/2$ would improve fringe visibility. Additionally, thermal cross-talk from the modulator termination reduces fringe visibility by changing the heat distribution across the chip, despite the global temperature set by the Peltier element and temperature controller. Improved heat sinking or recalibration of TPS

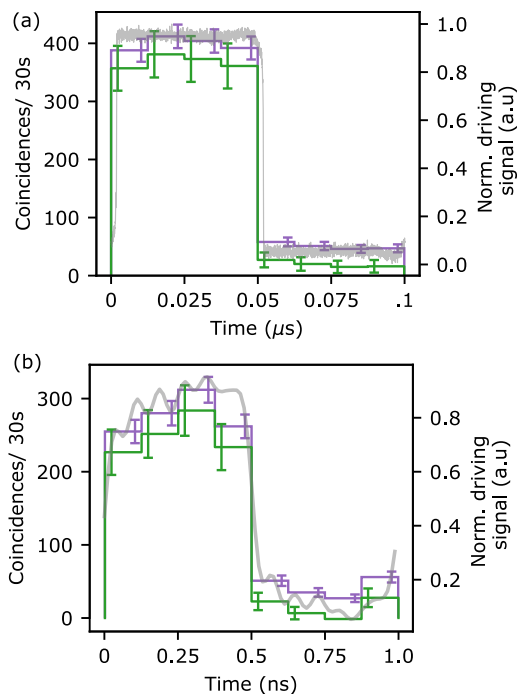


FIG. 4. Raw (purple) and background subtracted (green) coincidence counts from 10 MHz (a) and 1 GHz (b) square waves applied to the modulator (left axes). Timetag data is collected for 30 s while the modulation is applied, before postprocessing to identify coincidences. The peak to peak voltage of the modulator has been set at 3.95 V and 4.0 V, respectively, with a fixed DC bias of 2.1 V. The normalised driving waveform is overlaid in grey for comparison (right axes). Errors are calculated assuming Poissonian statistics.

while the CDM is operated could mitigate this effect.

In this work, we have demonstrated high speed modulation of nonlinear interferometry in silicon photonics to modulate photon pair generation at GHz speed. This does not expose the photon pairs generated to any parasitic loss of the CDM, and could allow for control over generation of other delicate quantum resources, without incurring insertion losses from high speed modulators. Because of the super-sensitive interference frequency of NLIs, the method enhances efficiency and reduces heat dissipation compared to modulation on the pump laser with a CDM at the input of the SOI chip. With the operation of silicon quantum photonics in the mid-IR [29], we anticipate on-chip NLIs can be combined with degenerate four wave mixing and mid-IR spectroscopy to detect greenhouse gas species on chip without needing mid-IR detectors [12]. Fast modulation of the interference effect could then be used to move the gas detection signal to a side band away from electronic noise sources. We also anticipate fast integrated NLIs to be a building block of more general nonlinear interferometric networks with increased capability for quantum applications over universal linear optics, such as scaling up large NLI super-

lattices [8], multiplexed sources [30] and quantum state engineering [9].

Acknowledgements and Contributions. We thank J. F. Tasker, A. Laing and Giacomo Ferranti for useful discussions. The authors are grateful for technical assistance from L. Kling. The experiment was conceived by T.O. and J.C.F.M. The PIC was designed by T.O. J.F. performed the experiment and data analysis, supervised by J.C.F.M. All authors contributed to writing the manuscript. J.F. acknowledges support from EPSRC Quantum Engineering Centre for Doctoral Training EP/L015730/1 and an EPSRC iCASE Thales studentship. J.C.F.M. acknowledges support from European Research Council starting grant ERC-2018-STG 803665 and a Philip Leverhulme Prize.

-
- [1] M. Reck, A. Zeilinger, H. J. Bernstein, and P. Bertani, Experimental realization of any discrete unitary operator, *Physical review letters* **73**, 58 (1994).
 - [2] J. Carolan, C. Harrold, C. Sparrow, E. Martín-López, N. J. Russell, J. W. Silverstone, P. J. Shadbolt, N. Matsuda, M. Oguma, M. Itoh, *et al.*, Universal linear optics, *Science* **349**, 711 (2015).
 - [3] H. Fukuda, K. Yamada, T. Shoji, M. Takahashi, T. Tsuchizawa, T. Watanabe, J.-i. Takahashi, and S.-i. Itabashi, Four-wave mixing in silicon wire waveguides, *Opt. Express* **13**, 4629 (2005).
 - [4] J. Bao, Z. Fu, T. Pramanik, J. Mao, Y. Chi, Y. Cao, C. Zhai, Y. Mao, T. Dai, X. Chen, X. Jia, L. Zhao, Y. Zheng, B. Tang, Z. Li, J. Luo, W. Wang, Y. Yang, Y. Peng, D. Liu, D. Dai, Q. He, A. L. Muthali, L. K. Oxenløwe, C. Vigliar, S. Paesani, H. Hou, R. Santagati, J. W. Silverstone, A. Laing, M. G. Thompson, J. L. O’Brien, Y. Ding, Q. Gong, and J. Wang, Very-large-scale integrated quantum graph photonics, *Nat. Photonics*, 1 (2023).
 - [5] M. Krenn, X. Gu, and A. Zeilinger, Quantum Experiments and Graphs: Multiparty States as Coherent Superpositions of Perfect Matchings, *Phys. Rev. Lett.* **119**, 240403 (2017).
 - [6] B. Yurke, S. L. McCall, and J. R. Klauder, SU(2) and SU(1,1) interferometers, *Phys. Rev. A* **33**, 4033 (1986).
 - [7] G. B. Lemos, V. Borish, G. D. Cole, S. Ramelow, R. Lapkiewicz, and A. Zeilinger, Quantum imaging with undetected photons, *Nature* **512**, 409 (2014).
 - [8] A. V. Paterova and L. A. Krivitsky, Nonlinear interference in crystal superlattices - Light: Science & Applications, *Light Sci. Appl.* **9**, 1 (2020).
 - [9] X. Gu, M. Erhard, A. Zeilinger, and M. Krenn, Quantum experiments and graphs II: Quantum interference, computation, and state generation, *Proc. Natl. Acad. Sci. U.S.A.* **116**, 4147 (2019).
 - [10] L. Cui, J. Su, J. Li, Y. Liu, X. Li, and Z. Ou, Quantum state engineering by nonlinear quantum interference, *Physical Review A* **102**, 033718 (2020).
 - [11] L.-T. F. Feng, M. Zhang, D. Liu, Y.-J. Cheng, G.-P. Guo, D.-X. Dai, G.-C. Guo, M. Krenn, and X.-F. Ren, On-chip quantum interference between the origins of a

- multi-photon state, *Optica* **10**, 105 (2023).
- [12] J. Lidner, Chiara amd Lunz, S. J. Herr, S. Wolf, J. Kießling, and F. Künemann, Nonlinear interferometer for Fourier-transform mid-infrared gas spectroscopy using near-infrared detection, *Optics Express* **29**, 4035 (2021).
- [13] T. Ono, G. F. Sinclair, D. Bonneau, M. G. Thompson, J. C. F. Matthews, and J. G. Rarity, Observation of non-linear interference on a silicon photonic chip, *Opt. Lett.* **44**, 1277 (2019).
- [14] J. W. Silverstone, J. Wang, D. Bonneau, P. Sibson, R. Santagati, C. Erven, J. O'Brien, and M. Thompson, Silicon quantum photonics, in *2016 International Conference on Optical MEMS and Nanophotonics (OMN)* (IEEE, 2016) pp. 1–2.
- [15] J. F. Tasker, J. Frazer, G. Ferranti, and J. C. F. Matthews, A bi-cmos electronic-photon integrated circuit quantum light detector, arXiv:2305.08990 (2023).
- [16] S. Paesani, M. Borghi, S. Signorini, A. Maïnos, L. Pavesi, and A. Laing, Near-ideal spontaneous photon sources in silicon quantum photonics, *Nature communications* **11**, 1 (2019).
- [17] N. C. Harris, Y. Ma, J. Mower, T. Baehr-Jones, D. Englund, M. Hochberg, and C. Galland, Efficient, compact and low loss thermo-optic phase shifter in silicon, *Opt. Express* **22**, 10487 (2014).
- [18] M. Jacques, A. Samani, E. El-Fiky, D. Patel, Z. Xing, and D. V. Plant, Optimization of thermo-optic phase-shifter design and mitigation of thermal crosstalk on the SOI platform, *Opt. Express* **27**, 10456 (2019).
- [19] U. Chakraborty, J. Carolan, G. Clark, D. Bunandar, G. Gilbert, J. Notaros, J. Notaros, M. R. Watts, D. R. Englund, and D. R. Englund, Cryogenic operation of silicon photonic modulators based on the DC Kerr effect, *Optica* **7**, 1385 (2020).
- [20] F. Kaneda, B. G. Christensen, J. J. Wong, H. S. Park, K. T. McCusker, and P. G. Kwiat, Time-multiplexed heralded single-photon source, *Optica* **2**, 1010 (2015).
- [21] R. Prevedel, P. Walther, F. Tiefenbacher, P. Böhi, R. Kaltenbaek, T. Jennewein, and A. Zeilinger, High-speed linear optics quantum computing using active feed-forward, *Nature* **445**, 65 (2007).
- [22] J. Wang, S. Paesani, R. Santagati, S. Knauer, A. A. Gentile, N. Wiebe, M. Petruzzella, J. L. O'Brien, J. G. Rarity, A. Laing, *et al.*, Experimental quantum hamiltonian learning, *Nature Physics* **13**, 551 (2017).
- [23] G. T. Reed, G. Mashanovich, F. Gardes, and D. Thomson, Silicon optical modulators, *Nature Photonics* **4**, 518 (2010).
- [24] G. T. Reed and C. E. Jason Png, Silicon optical modulators, *Mater. Today* **8**, 40 (2005).
- [25] G. T. Reed, G. Z. Mashanovich, F. Y. Gardes, M. Nedeljkovic, Y. Hu, D. J. Thomson, K. Li, P. R. Wilson, S.-W. Chen, and S. S. Hsu, Recent breakthroughs in carrier depletion based silicon optical modulators, *Nanophotonics* **3**, 229 (2014).
- [26] P. Sibson, J. E. Kennard, S. Stanisic, C. Erven, J. L. O'Brien, and M. G. Thompson, Integrated silicon photonics for high-speed quantum key distribution, *Optica* **4**, 172 (2017).
- [27] A. Rahim, J. Goyvaerts, B. Szelag, J.-M. Fedeli, P. Absil, T. Aalto, M. Harjanne, C. Littlejohns, G. Reed, G. Winzer, S. Lischke, L. Zimmermann, D. Knoll, D. Geuzebroek, A. Leinse, M. Geiselmann, M. Zervas, H. Jans, A. Stassen, C. Domínguez, P. Muñoz, D. Domenech, A. L. Giesecke, M. C. Lemme, and R. Baets, Open-Access Silicon Photonics Platforms in Europe, *IEEE J. Sel. Top. Quantum Electron.* **25**, 1 (2019).
- [28] J. E. Sharping, K. F. Lee, M. A. Foster, A. C. Turner, B. S. Schmidt, M. Lipson, A. L. Gaeta, and P. Kumar, Generation of correlated photons in nanoscale silicon waveguides, *Opt. Express* **14**, 12388 (2006).
- [29] L. M. Rosenfeld, D. A. Sulway, G. F. Sinclair, V. Anant, M. G. Thompson, J. G. Rarity, and J. W. Silverstone, Mid-infrared quantum optics in silicon, *Optics Express* **28**, 37092 (2020).
- [30] T. Rudolph, M. Thompson, J. Matthews, and D. Bonneau, Optical apparatus and method for outputting one or more photons (2018), uS Patent 9,952,482.